Systems/Circuits

Spontaneous Multimodal Neural Transmission Suggests That Adult Spinal Networks Maintain an Intrinsic State of Readiness to Execute Sensorimotor Behaviors

Maria F. Bandres,[1,5] Jefferson Gomes,[1] and Jacob G. McPherson[1,2,3,4,5]

[1]Program in Physical Therapy, [2]Department of Anesthesiology, [3]Washington University Pain Center, [4]Program in Neurosciences, Washington University in St. Louis School of Medicine, St. Louis, MO, 63108, and [5]Department of Biomedical Engineering, Washington University in St. Louis, St. Louis, MO, 63108

Spontaneous action potential discharge (spAP) is both ubiquitous and functionally relevant during neural development. spAP remains a prominent feature of supraspinal networks in maturity, even during unconsciousness. Evidence suggests that spAP persists in mature spinal networks during wakefulness, and one function of spAP in this context could be maintenance of a "ready state" to execute behaviors. The extent to which spAP persists in mature spinal networks during unconsciousness remains unclear, and its function(s), if any, are likewise unresolved. Here, we attempt to reconcile some of the questions and contradictions that emerge from the disintegrated picture of adult spinal spAP currently available. We recorded simultaneously from large populations of spinal interneurons *in vivo* in male rats, characterizing the spatial distribution of spAP in the lumbar enlargement and identifying subgroups of spontaneously active neurons. We find (1) concurrent spAP throughout the dorsoventral extent of the gray matter, with a diverse yet strikingly consistent mixture of neuron types across laminae; (2) the proportion of neurons exhibiting spAP in deeper, sensorimotor integrative regions is comparable to that in more superficial, sensory-dominant regions; (3) firing rate, but not spike train variability, varies systematically with region; and (4) spAP includes multimodal neural transmission consistent with executing a spinally-mediated behavior. These findings suggest that adult spAP may continue to support a state of readiness to execute sensorimotor behaviors even during unconsciousness. Such functionality has implications for our understanding of how perception is translated into action, of experience-dependent modification of behavior, and (mal)adaptative responses to injury or disease.

Key words: **interneuron; motor control; sensation; sensorimotor integration; spinal cord; spinal reflex**

Significance Statement

Neurons often discharge action potentials (APs) seemingly spontaneously, that is, in the absence of ongoing behaviors or overt stimuli. This phenomenon is particularly evident during neural development, where spontaneous AP discharge (spAP) is ubiquitous in the central nervous system and is crucial to establishing connectivity among functionally related groups of neurons. The function(s) of spAP in adult spinal networks, if any, have remained enigmatic, especially during unconsciousness. Here, we report evidence that one such function could be to support an intrinsic state of readiness to execute sensorimotor behaviors. This finding has implications for our understanding of how perception is translated into action, of experience-dependent modification of behavior, and (mal)adaptative responses to injury or disease.

Introduction

Spontaneous action potential discharge (spAP) is ubiquitous in the developing spinal cord, generating complex patterns of neural transmission necessary to link sensory inputs with motor outputs and shape nascent behaviors. For example, spAP in Lamina I neurons reinforces nociceptive flexion-withdrawal reflexes through monosynaptic actions on Lamina IX motoneurons (Baccei, 2014). The extent to which purposeful spAP persists in the adult spinal cord, particularly during unconsciousness, remains a central issue in understanding how perception is translated into action.

spAP in adult spinal networks has been interpreted as neuronal noise, a marker of tonic synaptic drive, and indicative of

Received Mar. 29, 2021; revised July 27, 2021; accepted July 30, 2021.

Author contributions: J.G.M. designed research; M.F.B., J.G., and J.G.M. performed research; M.F.B. and J.G.M. analyzed data; M.F.B. wrote the first draft of the paper; M.F.B. and J.G.M. edited the paper; M.F.B. and J.G.M. wrote the paper.

This work was supported by National Institutes of Health Grants K12HD073945 and 7R01NS111234-02 (to J.G.M.). We thank Dr. Gretchen A. Meyer for help with histological procedures and for providing access to microscopy supplies and equipment.

The authors declare no competing financial interests.

Correspondence should be addressed to Jacob G. McPherson at mcpherson.jacob@wustl.edu.

https://doi.org/10.1523/JNEUROSCI.0662-21.2021

pathology. And indeed, overly vigorous spAP could result in pain or involuntary movements and has been reported in conditions in which these symptoms manifest (Marcantoni et al., 2020; Thaweerattanasinp et al., 2020). However, spAP has also been reported in a range of adult spinal interneurons in the absence of neurologic injury (Cervero et al., 1979; Surmeier et al., 1989; Sandkühler and Eblen-Zajjur, 1994; Prut and Perlmutter, 2003; Borowska et al., 2013), and we and others have recently documented spontaneous functional connectivity among spinal networks during unconsciousness (Barry et al., 2014; Eippert et al., 2017; Wu et al., 2019; McPherson and Bandres, 2021). Together, these findings have led to speculation that spAP may continue to serve homeostatic, if enigmatic, functions.

One function of adult spinal spAP could be maintenance of an intrinsic state of readiness to execute sensorimotor behaviors. Presumably, this would require a combination of widespread concurrence throughout the gray matter and multimodal neural transmission, both in terms of firing patterns and phenomenological neuron types. These features are prominent in developing spinal networks, where the ability of spAP to facilitate specific behaviors is established (O'Donovan et al., 1998; Blankenship and Feller, 2010; Li and Baccei, 2011; Luz et al., 2014; Inácio et al., 2016). Systematic differences in discharge rates and spike train variability across regions of the gray matter would also be predicted, with the latter in particular potentially revealing additional clues about neural drive to spinal networks during unconsciousness and the mechanisms by which spAP modulates synaptic information transfer (Stevens and Zador, 1998; Svirskis and Rinzel, 2000).

Reports of the location and prevalence of spAP in the adult spinal cord are typically confined to restricted anatomic regions or functional networks (e.g., nociceptive), leaving its anatomic distribution unresolved. Differences in experimental preparation have led to further complications. For example, studies of deep spinal interneurons in anesthetized cats have reported only a minority of neurons exhibiting spAP (Rudomin et al., 1987; Bolton et al., 1991), whereas recordings in awake, behaving monkeys suggest that a majority of these neurons are spontaneously active (Prut and Perlmutter, 2003).

A curious picture has emerged from the available reports of spike train variability in spinal spAP. While reports of spAP in the dorsal horn indicate a high variability state with substantial bursting (Steedman and Zachary, 1990; Lucas-Romero et al., 2018), spAP in the intermediate gray matter (IG) and ventral horn (VH) appears to exhibit lower variability and minimal bursting (Prut and Perlmutter, 2003). In supraspinal networks, neuronal variability is advantageous for perception yet deleterious for action (Stein et al., 2005). It is unknown whether this principle generalizes to spinal spAP, particularly during unconsciousness. However, different effective states of variability would be consistent with this idea. Unfortunately, the robustness of this apparent finding cannot be inferred from the available literature because methodological differences between studies cross domains understood to alter spAP prevalence and variability.

Here, we attempt to reconcile some of the contradictions that emerge from our disintegrated understanding of adult spinal spAP. Using microelectrode arrays, we record simultaneously from large populations of spinal interneurons *in vivo* during unconsciousness and pose the following questions: (1) is spAP present throughout the gray matter of a spinal segment; (2) does spAP exhibit a preferential state of temporal variability; and (3) does the prevalence or variability of spAP differ across anatomic boundaries or neuron type?

Materials and Methods

A total of 18 adult male Sprague Dawley rats (290–500 g) were included in the study. Care and handling of animals conformed to protocols approved by the Institutional Animal Care and Use Committees of Florida International University and Washington University in St. Louis.

Surgical procedures

Inhaled isoflurane (~3.5–5% ISO in O_2, flow rate: ~0.9 l/min) was used for induction of anesthesia and urethane was used to maintain the anesthetized state for the remainder of the experiment. Urethane was administered as 1.2 g/kg, intraperitoneally, with boosts as necessary (0.2 g/kg, i.p.). Regarding choice of anesthetic agent, our previous work has indicated that the average absolute number of spontaneously active neurons accessible per rat is indistinguishable when using urethane versus isoflurane to achieve deep surgical anesthesia (McPherson and Bandres, 2021). However, two additional considerations informed our choice of urethane for these experiments.

One factor motivating our choice of urethane is that it produces a reasonable facsimile of natural sleep. There are several observations that support this conclusion. First, urethane preserves vital signs (i.e., heart rate, respiration rate, blood pressure, spO_2) within physiological norms (Maggi and Meli, 1986a,b; Daló and Hackman, 2013). Once a target plane of anesthesia is reached, vital signs can remain stable at these levels for hours without continuous infusion of drug, preventing the animal from becoming progressively more deeply anesthetized over the course of the experiment (Maggi and Meli, 1986c). By comparison, isoflurane markedly depresses vital signs, resulting in an atypical physiological state not directly comparable to natural sleep. Importantly, studies of supraspinal network activity also indicate that urethane-anesthetized animals transition between two states of unconsciousness that appear to be analogous to REM and NREM (slow wave) sleep (Lincoln, 1969; Clement et al., 2008; Zhurakovskaya et al., 2016, 2019). In addition to these electrophysiological changes, state transitions are also marked by changes in respiration rate (Pagliardini et al., 2012; Zhurakovskaya et al., 2019), which we routinely monitor during all experiments.

We also chose urethane specifically for its well documented suppression of spontaneous activity in the dorsal roots and its comparatively modest impact on membrane potential and neurotransmitter systems (including GABAergic and excitatory amino acid transmission; Maggi and Meli, 1986b; Hara and Harris, 2002; Daló and Hackman, 2013). Urethane also generally suppresses spontaneous dorsal horn activity more than VH activity, which is effectively the opposite gradient seen with isoflurane (Hara and Harris, 2002; Wakai et al., 2005; Grasshoff and Antkowiak, 2006; Kim et al., 2007; Daló and Hackman, 2013). Together, these features of urethane allow a measure of control over latent afferent inflow that would not otherwise be achievable with a fully intact preparation. Related to this point, we have previously demonstrated using epineurial lidocaine injections of the sciatic nerve that latent afferent transmission in our urethane preparation is negligible (McPherson and Bandres, 2021). And while mechanical deafferentation would wholly eliminate afferent inflow, it could paradoxically lead to non-physiological spontaneous discharge in dorsal horn neurons (Eschenfelder et al., 2000), confounding our interpretation of spAP.

When deep, surgical-plane anesthesia was achieved, a laminectomy was performed on the T13-L2 vertebrae overlaying the dorsal root entry zone of the L5 spinal nerve. We selected this spinal segment for two primary reasons. First, the lumbar enlargement contains sensorimotor networks known to exhibit spAP during development that are functionally relevant (e.g., establishing flexion withdrawal circuits). Thus, it is a logical comparator for adult spAP. Second, this spinal segment confers a practical benefit. Namely, that its corresponding dermatome is the glabrous skin of the hindpaw. This dermatome is advantageous both because the lack of hair limits unintended sensory feedback (e.g., slight brush of instrument on hair) and because it is readily accessible for

purposefully inducing sensory feedback (as during phenomenological classification of neurons exhibiting spAP).

Intact vertebrae rostral and caudal to the laminectomy were clamped with forceps in a custom, multi-degree-of-freedom frame and the animal was elevated slightly above the frame base to prevent upwards or downwards displacements in the spinal cord caused by respiration. Next, the frame and animal were transferred to an anti-vibration air table (Kinetic Systems, Inc.) surrounded by a Faraday cage. The exposed dura matter was incised rostrocaudally and the spinal cord bathed in homeothermic physiological ringer solution. Body temperature was continually monitored via rectal thermometer and regulated with a recirculating water heating pad. Heart rate, blood pressure, respiration rate, and SpO_2 were also monitored continually throughout the procedures (Kent Scientific). Lactated ringer solution was provided subcutaneously every 2 h to prevent dehydration. Animals were humanely euthanized at the end of experimentation via overdose of sodium pentobarbital consistent with American Veterinary Medical Association guidelines.

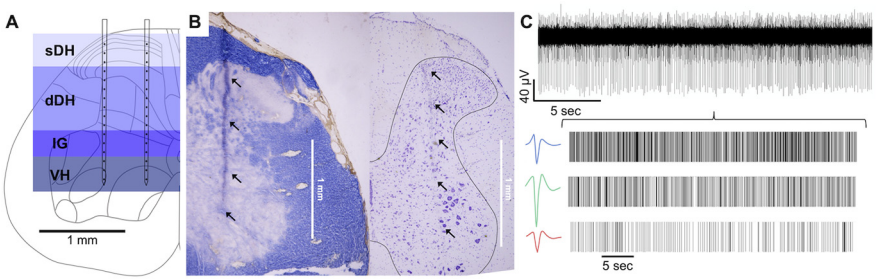

Figure 1. Experimental setup. ***A***, Schematic illustration of a transverse section of spinal segment L5 with an overlay of the implanted microelectrode array (dual-shank microelectrode arrays with 32 independent recording channels, arranged as 16 channels per shank). Locations for neuronal recording spanned the sDH, dDH, IG, and the VH. ***B***, Histologic verification of electrode placement. Left, Eriochrome cyanine R-stained section of a representative spinal segment with clear in-plane visualization of one electrode shank. Right, Adjacent cresyl violet-stained section indicating electrode track for one shank (gray matter border outlined for clarity). The large cell bodies adjacent to ventral-most black arrows are motoneurons of the crural flexor motor pool. ***C***, Each electrode recorded multiunit neural activity, which was discriminated offline into spike trains of spAP in individual neurons. Upper black trace, Spontaneous multiunit activity recorded from an electrode located in the dDH; colored waveforms and raster plots below represent spAP from three individual neurons discriminated from the above multiunit activity. Primary outcome measures from the data included the number and functional type of spontaneously active neurons, temporal features of spAP spike trains, and the spatiotemporal distribution of spAP throughout the gray matter.

For postmortem histology, fresh spinal cords were harvested and immediately frozen. Subsequently, the spinal cord was cut into 20-μm sections and stained either with cresyl violet or eriochrome cyanine R. Cresyl violet acetate (0.1%, pH 4.7) staining required 5 min at room temperature before differentiating in ethyl alcohol; eriochrome cyanine R staining required 10 min at room temperature before differentiating in 5% iron alum for 6 min followed by borax-ferricyanide differentiation also for 6 min.

Electrode implantation

We used planar 32-channel microelectrode arrays (NeuroNexus Inc.) to record neural transmission in the gray matter of the spinal cord. The arrays consist of two shanks, each with 16 individual electrodes (electrode area: 177 μm^2; interelectrode spacing: 100 μm; Fig. 1*A*, schematic overlay). The arrays were custom electrodeposited with activated platinum-iridium (Platinum Group Coatings) to increase charge capacity and to lower impedance (4–10 KΩ). Arrays were implanted with a custom 4-axis motorized micromanipulator with sub-micron resolution (Siskiyou Corp.).

For insertion into the spinal cord, the microelectrode array was oriented perpendicular to the midline and positioned over the L5 dorsal root entry zone (viewed under high magnification). Confirmation of initial localization was then assessed by recording dorsal root potentials from the surface of the spinal cord while mechanically probing the glabrous skin of the plantar surface of the hindpaw (i.e., the L5 dermatome). If dorsal root potentials were synchronous with dermatome mapping, electrode insertion commenced; if clearly correlated dorsal root potentials were not visible, the insertion site was adjusted accordingly.

Subsequently, the microelectrode array was lowered through the pia mater and into the neural tissue. The array was lowered slowly, in ~25-μm increments, to avoid excessive shear or planar stress on the tissue. Concurrently, we mechanically probed the hindpaw while visualizing in real-time multiunit neural activity from the array to ensure that the insertion site continued to closely track the desired dermatome. When the ventral-most electrodes reached a depth of ~400–500 μm, corresponding to the deep dorsal horn (dDH), we mapped their specific receptive fields to ensure accurate placement. If, at this depth, the receptive field had either shifted (e.g., to the ankle) or if multiunit data with an appropriate signal-to-noise ratio was not found, the electrode was removed from the cord and re-tracked. If an appropriate receptive field and signal-to-noise was achieved at this depth, the electrode array was inserted fully such that all recording sites were below the surface of the spinal cord and the ventral most electrodes were ~1600–1800 μm deep to the surface. Electrodes were not moved after achieving the target depth. We subdivided the microelectrode array into gross anatomic regions corresponding approximately to the superficial dorsal horn (sDH; ~100–300 μm), the dDH (~400–1000 μm), the IG (~1100–1300 μm), and the VH (~1400–1600+ μm; Fig. 1*A*).

Additional measures of electrode placement were as follows. After the reaching our target implant depth, we characterized motor threshold by stimulating through the ventral-most and lateral-most electrode. Single-pulse current thresholds of ~5–15 μA to evoke flexion of the ipsilateral toes was considered an additional level of intraoperative verification of microelectrode array placement. We also monitored the microdrive depth during electrode explant. Differences between implant and explant depth presumably reflected tissue deformation during the experiment (e.g., compression during initial penetration, creep during recording) and were used as a correction factor for estimating electrode depth. Finally, we performed histologic analyses of spinal sections after the conclusion of the experiments (Fig. 1*B*). Electrode tracks (or portions thereof) were visible on many, but not all, of the sections. Electrode track visibility was the limited by two main factors: the small size of the electrode shanks themselves and the lack of tissue damage introduced by the implant procedure. Commonly, we found that only a single shank was visible in-plane on a given section (Fig. 1*B*), because of slight deviations between the implant and cutting angles. Together, we estimate that electrode depth varied by $\leq$100 μm per rat.

Electrophysiological recordings and analyses

The microelectrode array was coupled to a Nano2+Stim headstage (Ripple Neuro) and broadband data were sampled at 30 KHz. Extracellular multiunit neural activity (Fig. 1*C*, top panel) was recorded in trials with epochs of spontaneous neural transmission and trials containing epochs with periods of nociceptive and/or non-nociceptive (NN) sensory afferent transmission. Sensory afferent transmission was induced for 1–5 s every ~20–30 s via mechanical probing of the L5 dermatome. Nociceptive transmission was induced by firmly pinching the most sensitive receptive field of the plantar surface of the ipsilateral hindpaw using precision forceps (FST). NN cutaneous transmission was induced by gently touching or brushing the same region with a cotton-tipped applicator. Acquisition order was randomized, and each epoch lasted between 30 s and 5 min. Experimental sessions lasted up to 6–10 h total, from anesthetic induction to euthanasia and tissue harvesting. The typical elapsed time between the initial reflection of the dura mater and conclusion of the electrophysiological recording session was 2–4 h.

Raw multiunit neural data (Fig. 1*C*, top panel) were processed using customized algorithms in MATLAB (The MathWorks). Initial clustering and extraction of single unit activity was achieved through a previously validated wavelet-based spike sorting algorithm (Quiroga et al., 2004; Fig. 1*C*, colored spike waveforms and associated raster plots). For each trial, we further verified the discrimination by removing neurons with non-physiological waveform shape, inappropriate AP durations, or interspike intervals (ISIs) less than the nominal refractory time. We paid particular attention to neurons discriminated on the same or on adjacent electrodes to identify and resolve instances of duplication. Neurons with an average firing rate <0.1 Hz over the duration of a trial were not considered to exhibit spAP. The number of spontaneously active neurons per animal was defined as the average number of spontaneously active neurons per trial; the total number of active neurons across all animals was taken as the sum of the per-animal averages.

Spike trains of spontaneously active neurons were classified into four firing type subgroups based on their regularity and the presence of bursting: regular simple (RS), irregular simple (IS), regular bursting (RB), and irregular bursting (IB; adapted from Lucas-Romero et al., 2018). Regularity was measured by the coefficient of variation (CV) of the ISIs. The CV is defined as the ratio of the standard deviation of the ISIs to the mean ISI; a lower CV implies a more regular firing. The threshold to classify a neuron as regular firing was CV < 0.5 (Rees et al., 1997). Spike trains were also assessed by the percentage of spikes clustered in bursts. A neuron was included in a bursting subgroup if $>25\%$ spikes were clustered in bursts, where a burst was defined as more than or equal to two consecutive spikes with an instantaneous firing frequency (IFF) greater than a threshold defined by the mean discharge rate of the neuron across the trial. Burst duration was taken as the elapsed time between the first spike whose IFF was above the frequency threshold and the last spike whose IFF was above the frequency threshold. Assignment of neurons to the RB versus IB subgroups was determined by the CV of interburst intervals.

Experimental design and statistical analyses

Sample size determination is a complex process for data and analyses such as ours. The number of animals per cohort, as is frequently taken to be the requisite sample size, is not the most appropriate measure of sample size for our study design. The ability to make statistical inferences about our primary outcome measures (e.g., proportion of neurons within a region or gaining membership into a specific subgroup) is based on the number of well-isolated neurons we are able to access per animal, per trial, per electrode. Microelectrode array recordings inherently undersample the overall population of neurons, which is itself unknowable in absolute numbers. This limitation is particularly noteworthy in *in vivo* preparations, and is certainly present in our approach. In recognition of this sampling issue, however, we focused on the relative proportion of neurons within regions or gaining membership into specific subgroups. In this way, our statistical measures are controlled by a "within array" design, analogous to a case series study. We make no attempts to generalize to other states or conditions, for which a comparison cohort or further intervention would be required for statistical inference.

Based on our previous work using these microelectrode arrays, we anticipated that we could reliably discriminate ~50–60 neurons per trial, per animal (McPherson and Bandres, 2021; see Results). To estimate whether this total would potentially be sufficient to make inferences about our primary outcome measures within an animal, we adapted standard sample size estimation measures used in epidemiological prevalence studies (Daniel and Cross, 2013). Specifically, the number of spontaneously active neurons per trial, n, can be estimated as $n = Z^2 * P(1-P)/d^2$, where Z is the confidence level, P is the anticipated prevalence, and d is the precision of measurement. Confidence level Z was fixed at 95%. We nominally took P to be 25% for the purposes of estimation, which would represent uniformly distributed membership across subgroups given that we have four primary subgroups for the majority of our outcomes, e.g., spinal region, subgroups by firing type, subgroups by phenomenological classification. And lastly, we allowed d to range from 5–10%. Together, these parameters indicated the need to access between 17 and 68 spontaneously active neurons per trial.

Specific statistical analyses then proceeded as follows. The number and proportion of neurons exhibiting spAP per subgroup (e.g., anatomic region, firing type, phenomenological type) was assessed using one-way repeated-measures ANOVA models with the specific subgroup (e.g., region) as the repeated measure. Greenhouse–Geisser correction was applied if the assumption of sphericity was violated.

For analyses of potential relationships between firing rate metrics and region, as well as for CV and region, we treated region as a continuous numerical variable rather than as categorical (i.e., based on electrode depth from surface in micrometers, not coded as sDH, dDH, IG, VH). For these analyses, we used linear regression models rather than the ANOVA construct. Our primary outcome measure in these analyses was the strength and direction of the overall trend of a given parameter across depth, not whether a single depth was necessarily different from an adjacent depth. This choice was made for several reasons: (1) the gross anatomic regions we defined are a product of the electrode geometry we used and our placement of the electrodes in the spinal cord, which is not a standardized across the literature; (2) minute variations in electrode placement per rat could have introduced variability not captured using categorical approaches; and (3) investigators using different strains of rats, segments of the spinal cord, or different species would not be able to directly translate pairwise comparisons of differences. Independent tests of mean firing rate or CV differences between two groups used two-tailed, unpaired t tests.

We also sought to determine whether rat-level subgroups rather than (or in addition to) neuron-level subgroups were evident. These analyses included two phases. In the first, we constructed linear mixed models to determine the potential effect of rat-level factors on the following relationships: (1) anatomic region and the proportion of neurons exhibiting spAP; (2) firing type and the proportion of neurons exhibiting spAP; and (3) phenomenological neuron type and proportion of neurons exhibiting spAP. In each model, rat was included as a random factor with an intercept. Next, we performed a k-means cluster analysis ("squared Euclidean" distance measure) for bursting neurons, including the following nine parameters: anatomic region, interburst CV, intraburst CV, mean number of spikes per burst, mean interburst frequency, mean intraburst frequency, mean burst duration, overall mean firing rate, and mean instantaneous firing rate. Rat was used a grouping variable to determine whether clusters identified at the neuron-level were indeed subgrouped across animals. The number of clusters to range from two to five.

Statistical results were nominally considered significant at the $\alpha = 0.05$ level; Bonferroni correction was used to control family-wise error rate for *post hoc* testing as needed. Statistical analyses were performed in the MATLAB (The MathWorks) and SPSS Statistics (IBM) environments. Data in text and error bars on figures are presented as mean ± SE unless otherwise noted.

Results

We identified an average of 50 (±5) well-isolated spontaneously active neurons per trial across all animals. With extracellular microelectrode array recordings such as ours, it is not possible to determine unequivocally the number of neurons from which we recorded. Indeed, some of the neurons, but presumably not all, exhibited spAP during multiple trials (whether consecutive or not) for each animal. Thus, we estimate the possible range of recorded neurons across the cohort to be from ~550 neurons (i.e., 50 neurons/animal × 11 animals) to ~4000 neurons (taking each neuron per trial as independent).

Neurons exhibiting spAP during unconsciousness are widely distributed throughout sensory and motor regions of the gray matter

It has remained unclear whether and how the proportion of neurons exhibiting spAP differs across anatomically and functionally delineated regions of the spinal gray matter. To address this question, we quantified the prevalence of spAP by anatomic

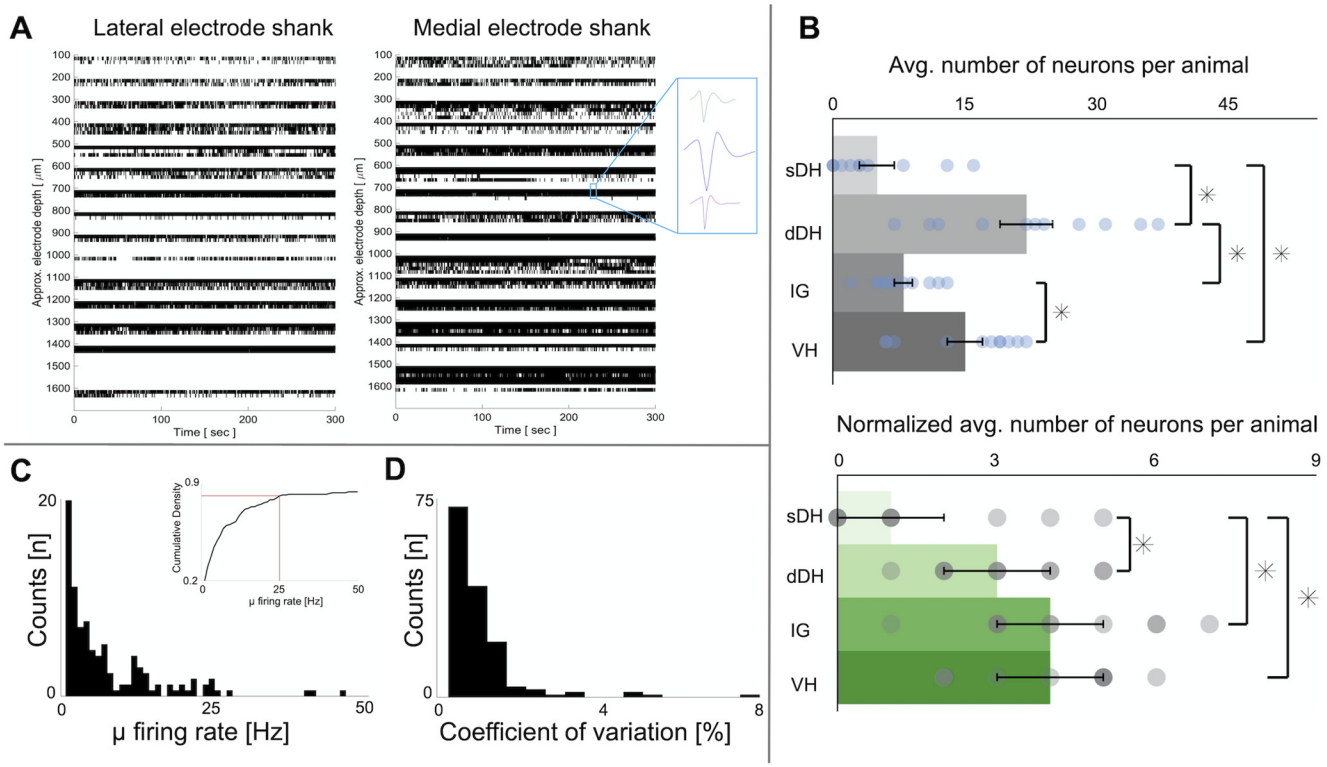

Figure 2. Spontaneous neural transmission throughout the dorsoventral extent of the gray matter of the spinal cord. ***A***, Representative raster plot of spontaneously active neurons from one rat; rows represent discrete neurons (lateral shank: 36 neurons; medial shank: 39 neurons). The abscissas in both plots (time) are synchronized. Inset depicts spike waveforms discriminated from a single electrode. ***B***, gray, top, Average number of spontaneously active neurons per gross anatomic region across animals (mean ± SEM; $n = 11$ animals, blue dots). There was an overall main effect of region on the proportion of spontaneously active neurons ($F = 21.579$, $p \ll 0.001$, $\eta^2 = 0.683$). Significant differences were also found between anatomic regions: dDH to sDH ($p \ll 0.0001$), dDH to IG ($p = 0.001$), VH to sDH ($p = 0.016$), and VH to IG ($p = 0.001$). Green bars, bottom, Average number of spontaneously active neurons normalized by the number of channels in the anatomic area (mean ± SEM; $n = 11$ animals, gray dots). When normalized, the number of spontaneously active neurons in the dDH, IG, and VH is significantly higher than the number of neurons in the sDH (overall main effect of region, $F = 9.788$, $p \ll 0.001$; $\eta^2 = 0.495$; sDH vs dDH, $p = 0.028$; sDH vs IG, $p = 0.012$; sDH vs VH, $p = 0.043$; all other pairwise comparisons are non-significant). ***C***, Histogram of overall mean firing rates of spontaneously active neurons from all animals; inset depicts cumulative density. In total, ~80% of all neurons had a firing rate ≤25 Hz (red lines, inset) when not considering firing type subgroups. ***D***, Histogram of the CV of all spontaneously active neurons from all animals.

region. A representative raster plot of spAP from one trial is shown is Figure 2*A*. Robust spAP was observed throughout the dorsoventral extent of the gray matter. The interlaminar distribution of spontaneously active neurons per animal was as following: sDH, 5 ± 2; dDH, 22 ± 3; IG, 8 ± 1; and VH, 15 ± 2 (Fig. 2*B*, gray bars). We found an overall main effect of anatomic region on the proportion of neurons exhibiting spAP ($F = 21.579$, $p \ll 0.001$; $\eta^2 = 0.683$), driven by a significantly increased prevalence of spAP in the dDH and VH relative to the sDH and IG (dDH to sDH, $p \ll 0.0001$; dDH to IG, $p = 0.001$; VH to sDH, $p = 0.016$; and VH to IG, $p = 0.001$). The dDH contained the highest proportion of neurons exhibiting spAP, at ~45%, followed by the VH, at ~31%, the IG (~15%), and the sDH (~9%). After normalizing for anatomic area, however, the prevalence of spAP in the dDH, IG, and VH was statistically indistinguishable, and all were greater than the sDH (overall main effect of region, $F = 9.788$, $p \ll 0.001$; $\eta^2 = 0.495$; sDH vs dDH, $p = 0.028$; sDH vs IG, $p = 0.012$; sDH vs VH, $p = 0.043$; all other pairwise comparisons are non-significant; Fig. 2*B*, green bars). We found no rat-level subgroups in the distribution of spAP across regions (Wald Z statistic = 1.460, $p = 0.144$).

spAP contains a diverse mixture of neuron subgroups defined by firing patterns

Across the entire population of neurons exhibiting spAP, the mean firing rate was 7.1 ± 0.64 Hz (Fig. 2*C*). The distribution of firing rates was asymmetrical and heavily skewed toward low frequencies. In total, ~80% of all neurons had a firing rate ≤25 Hz (Fig. 2*C*, inset). We found no systematic differences in firing rate across anatomic regions when pooling all neurons and examining only mean firing rate, although the dDH and VH were more likely to contain secondary peaks in the 10- to 15-Hz range (Fig. 2*C*). The mean CV across the population was 1.39 (Fig. 2*D*).

The presence of potential secondary peaks in the distribution of mean spAP firing rate (e.g., between ~10 and 15 Hz), coupled with previously published reports (Fetz et al., 2002; Lucas-Romero et al., 2018), strongly suggested that subgroups of interneurons may exist within our population based on specific discharge patterns. Such a finding could reflect ongoing multimodal neural transmission (Thaweerattanasinp et al., 2016). To investigate this possibility, we used temporal features of the spAP spike trains, including their variability, to delineate four firing type subgroups: IS, RS, IB, and RB (see Materials and Methods; Lucas-Romero et al., 2018). A representative example of each subgroup is shown in Figure 3. Autocorrelation functions and ISI histograms for neurons in each subgroup were consistent with their canonical forms [e.g., periodicity in RS neurons (Fig. 3*A*); similar to a Poisson process for IS neurons (Fig. 3*B*)]. Although not surprising, the finding of clear subgroups is consistent with the non-Gaussian distribution of mean frequencies seen across the population (Fig. 2*C*).

The proportion of neurons belonging to each subgroup was not uniform (overall main effect of region, $F = 56.383$; $p \ll 0.001$;

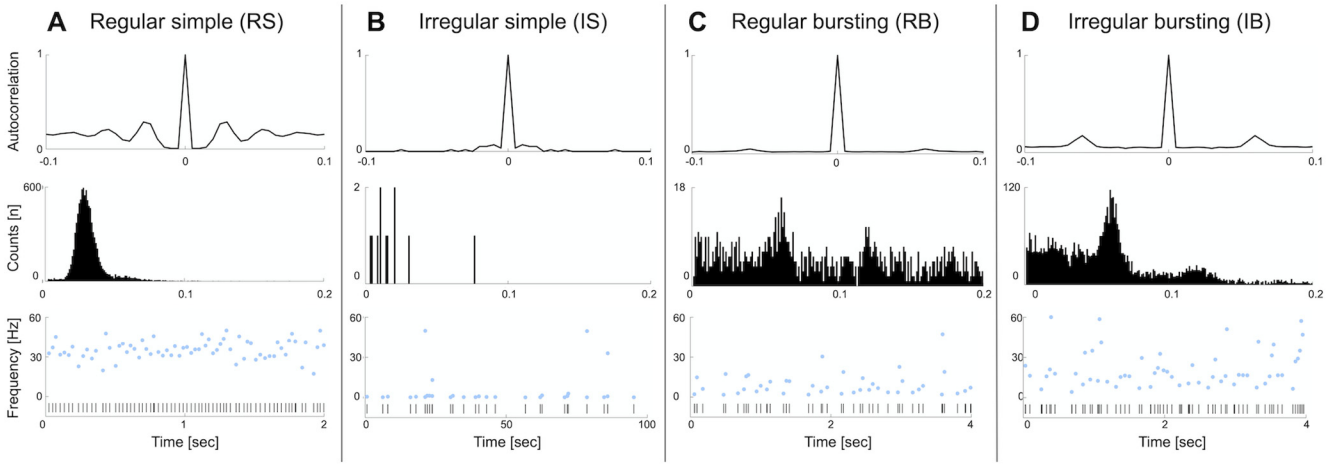

Figure 3. Neuron subgroups by firing type. Neurons exhibiting spAP were classified either as RS, IS, RB, or IB. ***A–D***, Representative examples of spAP from each subgroup. From top to bottom, each subplot depicts: the spAP autocorrelation function (upper figure); histogram of spAP ISIs (middle figure); and the IFF (blue dots) and raster plot (vertical dashes) for segment of time (note: time scales vary per subplot). Autocorrelation functions and ISI histograms for neurons in each subgroup were consistent with their canonical forms [e.g., periodicity in RS neuron autocorrelation (***A***); Poisson process-like autocorrelation in IS neurons (***B***); secondary peaks indicative of burstiness in ***C***, ***D***].

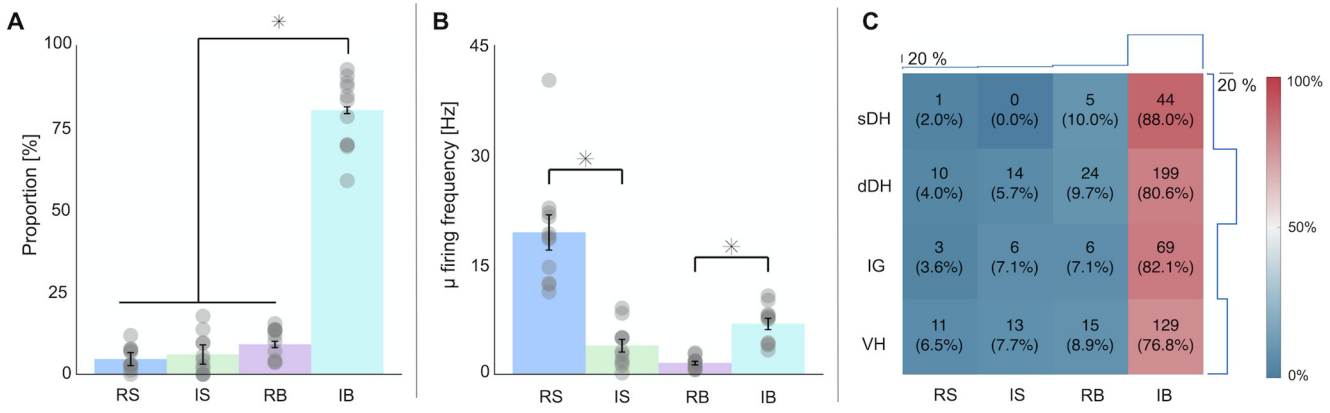

Figure 4. Distribution of spontaneously active neurons classified by temporal discharge patterns. ***A***, Proportion of spontaneously active neurons by firing subgroup across all animals (mean ± SEM; $n = 11$, gray dots), independent of anatomic region. Overall main effect of region ($F = 56.383$; $p \ll 0.001$; $\eta^2 = 0.825$), driven by IB, which was significantly greater than all other regions ($p \ll 0.0001$ for all comparisons; no other regions were statistically distinguishable from one another). ***B***, Mean firing rate of each firing type subgroup across all anatomic locations and animals (mean ± SEM; $n = 11$, gray dots). IS firing neurons exhibited a lower mean firing rate than RS firing neurons (3.92 ± 0.86 vs 19.42 ± 2.42 Hz; $p \ll 0.001$, $d = 1.707$), whereas IB firing neurons exhibited a higher firing rate than RB neurons (6.89 ± 0.77 vs 1.54 ± 0.24 Hz; $p \ll 0.001$, $d = 1.404$). ***C***, Heat map of firing types by anatomic region in the gray matter. Stair lines on the top represent the percentage of each firing type (i.e., the sum of columns). The IB firing type was the most prevalent type in all regions. Stair lines to the right represent the proportion of spAP neurons in each anatomic region (i.e., sum of rows). The dDH contained the greatest number of spontaneously active neurons. Percentage values indicated inside the heatmap squares represent the proportion of a given neuron type within that anatomic region (e.g., 2% of spAP neurons in the sDH were of the RS type).

$\eta^2 = 0.825$). Interestingly, ~80% belonged to the IB subgroup ($p \ll 0.0001$ for comparisons of IB mean to each other region; Fig. 4*A*). RB neurons comprised an additional 9% of the population, while IS and RS neurons comprised ~6% and ~5%, respectively (no significant differences in mean proportion between RS, IS, and RB; Fig. 4*A*). The total proportion of bursting neurons, 89% (including IB and RB), was significantly higher than the total proportion of simple firing neurons, at 11% (IS and RS; $p \ll 0.001$). The marked overrepresentation of bursting neurons was not expected based on the available literature, which has suggested both quantitatively and anecdotally that IS and RS subgroups are dominant in intraspinal spAP (Cervero et al., 1979; Prut and Perlmutter, 2003; Roza et al., 2016; Lucas-Romero et al., 2018). The predominance of bursting neurons could not be explained by rat-level subgroups, which were not evident for (rat-level variance in linear mixed model ≪0.001; Wald's Z not calculable).

The mean firing rates of neurons in each subgroup are presented in Figure 4*B*. Here, another intriguing observation emerges. Whereas IS neurons have a lower mean firing rate than RS neurons (3.92 ± 0.86 vs 19.42 ± 2.42 Hz; $p \ll 0.001$; $d = 1.707$), IB neurons have a higher firing rate than RB neurons (6.89 ± 0.77 vs 1.54 ± 0.24 Hz; $p \ll 0.001$; $d = 1.404$). Intraburst and interburst frequencies were likewise higher for the IB subgroup than the RB subgroup (22.07 ± 1.25 and 0.56 ± 0.03 Hz vs 15.58 ± 2.74 and 0.27 ± 0.02 Hz, respectively). Thus, neither spAP regularity nor the presence of spontaneous bursting alone appears to be capable of adequately predicting relative firing rate (i.e., higher vs lower rate).

We then quantified the anatomic distribution of firing type subgroups (Fig. 4*C*). All subgroups were detected in each region of the gray matter with the exception of the IS firing subgroup, which was nearly absent in the sDH. The IB subgroup, already the most prevalent when pooling across all anatomic regions,

was also the most prevalent subgroup within each individual region. The proportion of IB neurons in each region was relatively uniformly distributed, at ~80%. No other subgroup exceeded 10% of the total number of identified neurons in a given region. Taken together, bursting neurons (IB, RB) were markedly overrepresented compared with simple firing neurons (IS, RS) in each region of the cord. We found no clear relationships between region of the spinal cord and the relative proportion of a given neuron subgroup.

Firing rate is unreliably linked to spike train variability across spAP subgroups and is differentially modified by anatomic region

Rate and temporal coding are both widely acknowledged to be distinct, yet complementary, mechanisms by which information can be transmitted across a synapse. It has also been established that the temporal variability of a neuron's spike train depends on the relative synchrony of its inputs (Stevens and Zador, 1998). In this context, relationships between firing rate and temporal variability can provide additional information about the mechanisms by which subgroups of neurons tend to convey information.

Plots of CV versus firing rate can be seen in Figure 5. In Figure 5*A*, all neurons are shown, pooled across all trials, rats, and firing type subgroups; the CVs and firing rates of neurons belonging to bursting subgroups are computed without regard to clustering in bursts. The data nominally appear to follow an inverse relationship between CV and firing rate, which is consistent with previous reports of diverse pools of spinal interneurons (Prut and Perlmutter, 2003). However, this relationship belies the fundamentally different CV–firing rate relationships of its constituent subgroups (Fig. 5*B*,*C*).

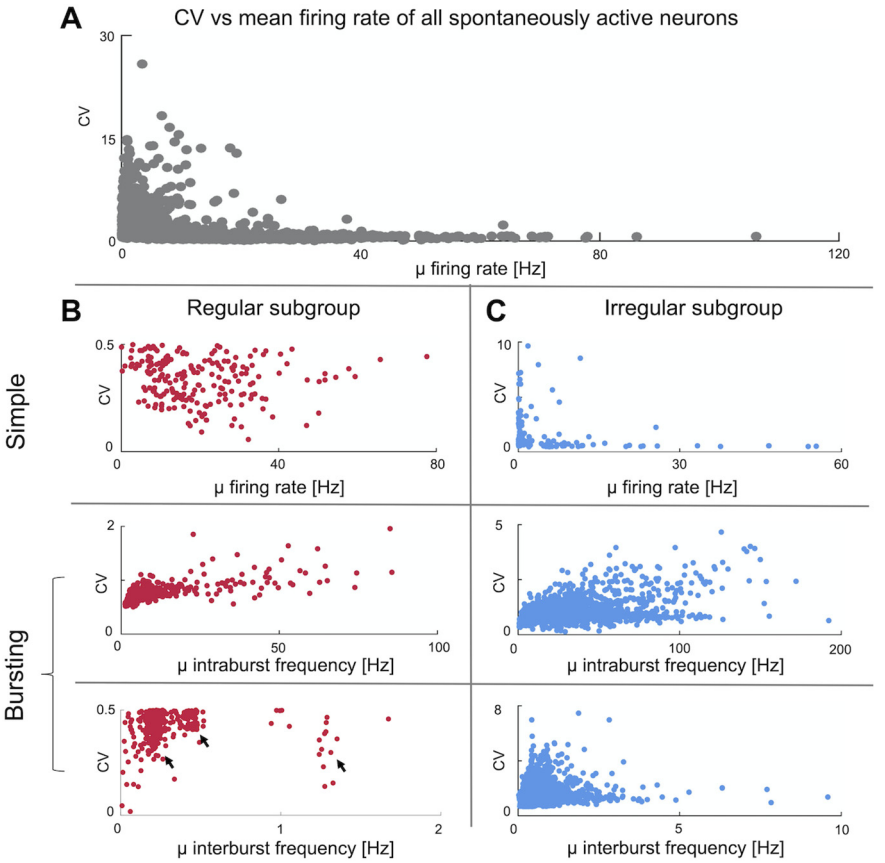

Figure 5. CV and firing rate are not consistently related across firing type subgroups. ***A***, All spontaneously active neurons across all animals and firing type subgroups (4072 neurons). Note: bursting is not considered in this plot; CV and firing rate are computed as if ISI are continuously distributed rather than clustered. The apparent inverse relationship between CV and firing rate masks the complex behavior of individual neuron subgroups (***B***, ***C***). ***B***, CV versus firing rate for regular firing neurons. The first row corresponds to CV and mean firing rate of RS neurons; the second row depicts CV and intraburst firing rate of RB neurons; the third row depicts CV and interburst frequency for RB neurons. Interburst frequencies in the RB population formed three distinct clusters (black arrows), at ~0.2, ~0.4, and ~1.3 Hz. ***C***, CV versus firing rate for irregular firing neurons. The first row corresponds to CV and mean firing rate of IS neurons; the second row depicts CV and intraburst firing rate of IB neurons; and the third row represents the CV and interburst frequency of IB neurons.

Although first or second order polynomials, power, and exponential functions are often used to relate CV and firing rate, we found that these models were relatively poorly conditioned for describing the observed data. For example, the most effective linear models fit the RB and IB subgroups, where changes in intraburst firing rate could explain 58% and 25% of the variance in intraburst CV, respectively (Fig. 5*B*,*C*, middle rows, both $p \ll 0.001$). Changes in interburst frequency could explain 7.5% of changes in interburst CV for the IB subgroup ($p \ll 0.001$; Fig. 5*C*, bottom row), the only other subgroup to exhibit a significant linear relationship. Linear relationships could explain $\leq$~1% of variability in the IS, RS, and RB-interburst subgroups (all nonsignificant).

The dispersion of firing rates and CVs was effectively continuous throughout their available ranges for all CV–firing rate relationships. The lone exception was for CV and interburst frequency in the RB subgroup (Fig. 5*B*, bottom row), where interburst frequencies formed three distinct clusters, at ~0.2, ~0.4, and ~1.3 Hz (Fig. 5*B*, bottom row, arrow annotations). The potential physiological significance of these clusters is unclear, although synchrony in this general frequency range has previously been observed in intrinsic spinal networks (Lucas-Romero et al., 2018), intrinsic supraspinal networks (Steriade et al., 1993), and descending neural drive (De Luca and Erim, 1994; Negro et al., 2016).

We then asked whether the temporal properties of spAP varied systematically as a function of anatomic region (Fig. 6). Two firing rate patterns emerged, revealing further distinctions between the simple firing and bursting subgroups. Across the simple firing subgroups, estimates of mean firing rate were independent of anatomic region (Fig. 6*A*, top panel), and RS neurons in each region exhibited higher mean frequencies than IS neurons in the same regions (Fig. 6*A*, asterisks indicate significant pairwise comparisons between RS and IS neurons, as follows: sDH, $p = 0.002$, $d = 2.912$; dDH, $p = 2.68\text{e-}6$, $d = 2.636$; IG, $p = 0.004$, $d = 1.171$; VH, $p = 3.27\text{e-}5$, $d = 2.092$; significant p value corrected to 0.0125 to control family-wise error rate). In contrast, estimates of firing rate for the bursting subgroups increased with increasing depth (i.e., from dorsal most to ventral most) except for the overall mean and intraburst firing rates for the RB

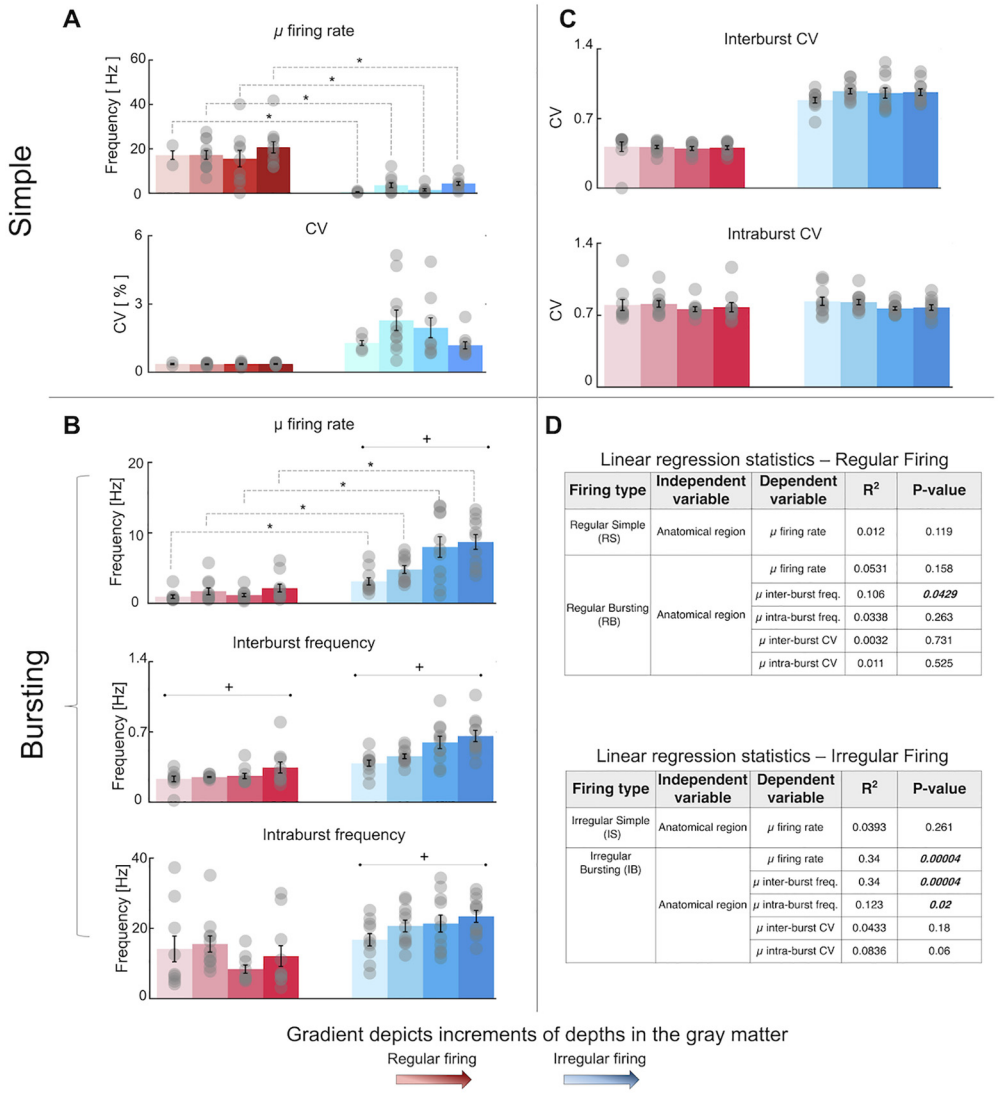

Linear regression statistics – Regular Firing

Firing type	Independent variable	Dependent variable	R^2	P-value
Regular Simple (RS)	Anatomical region	μ firing rate	0.012	0.119
Regular Bursting (RB)	Anatomical region	μ firing rate	0.0531	0.158
		μ inter-burst freq.	0.106	***0.0429***
		μ intra-burst freq.	0.0338	0.263
		μ inter-burst CV	0.0032	0.731
		μ intra-burst CV	0.011	0.525

Linear regression statistics – Irregular Firing

Firing type	Independent variable	Dependent variable	R^2	P-value
Irregular Simple (IS)	Anatomical region	μ firing rate	0.0393	0.261
Irregular Bursting (IB)	Anatomical region	μ firing rate	0.34	***0.00004***
		μ inter-burst freq.	0.34	***0.00004***
		μ intra-burst freq.	0.123	***0.02***
		μ inter-burst CV	0.0433	0.18
		μ intra-burst CV	0.0836	0.06

Figure 6. Firing rate, but not CV, varies with anatomic region in the gray matter. In all bar plots, red bars depict regular firing subgroups (RS and RB), and blue bars depict irregular firing subgroups (IS, IB). Color gradients in all plots depict depth in the gray matter; from lightest to darkest: sDH (first bar), dDH (second bar), IG (third bar), VH (fourth bar). All bar plots presented as mean ± SEM ($n = 11$, gray dots). ***A***, Spatiotemporal firing metrics as function of anatomic region for simple firing neurons (RS and IS): overall mean firing rate (top) and CV (bottom). ***B***, Spatiotemporal firing metrics as function of anatomic region for bursting neurons (RB and IB). ***C***, Interburst CV (top) and intraburst CV (bottom). ***D***, Linear regression statistics for each subgroup and parameter as indicated. Dashed lines and asterisks indicate significant pairwise comparisons between regular and irregular groups at a given anatomic region; solid lines with crosses indicate significant overall relationship within a group versus anatomic region (e.g., RB interburst frequency vs anatomic region).

subgroup (Fig. 6*B*). In addition, RB neurons exhibited lower mean frequencies in each region than co-located IB neurons (Fig. 6*B*, top panel; asterisks indicate significant pairwise comparisons between RB and IB neurons, as follows: sDH, $p = 0.005$, $d = 1.082$; dDH, $p = 3.83\text{e-}5$, $d = 1.935$; IG, $p = 0.0014$, $d = 1.709$; VH, $p = 0.0002$, $d = 1.739$; significant p value corrected to 0.0125 to control family-wise error rate). These observations were consistent with the pooled data across all anatomic regions, described previously. Unlike firing rate, and contrary to predictions from the literature, measures of CV were invariant to anatomic region for all subgroups (Fig. 6*A*,*C*). Summary data from the regression analyses is tabulated as in Figure 6*D*.

Unconscious spAP includes persistent multimodal neural transmission

Although neurons transmitting different modalities of sensorimotor information often exhibit characteristic discharge patterns and/or localize in different anatomic regions, these are indirect measures of the diversity of information being transmitted. A more direct way to detect the presence of ongoing multimodal neural transmission is to phenomenologically characterize changes in firing dynamics in response to known stimuli. Under the working hypothesis that spinal networks may maintain an intrinsic state of readiness to execute sensorimotor behaviors, we reasoned that transmission of nociceptive and NN cutaneous information would likely be a component of spAP. To test this hypothesis and to control for the potential confound of indirect measures of the types of information being transmitted, we attempted to determine the phenomenological type of neurons in our sample based on their evoked responses to mechanical probing of the L5 dermatome.

We tracked neurons known to exhibit spAP throughout recording epochs that also included (separately) periods of noxious and innocuous cutaneous stimuli. We then classified the neurons as follows: NN if firing rate increased during periods of innocuous but not noxious stimulation; wide dynamic range (WDR) if

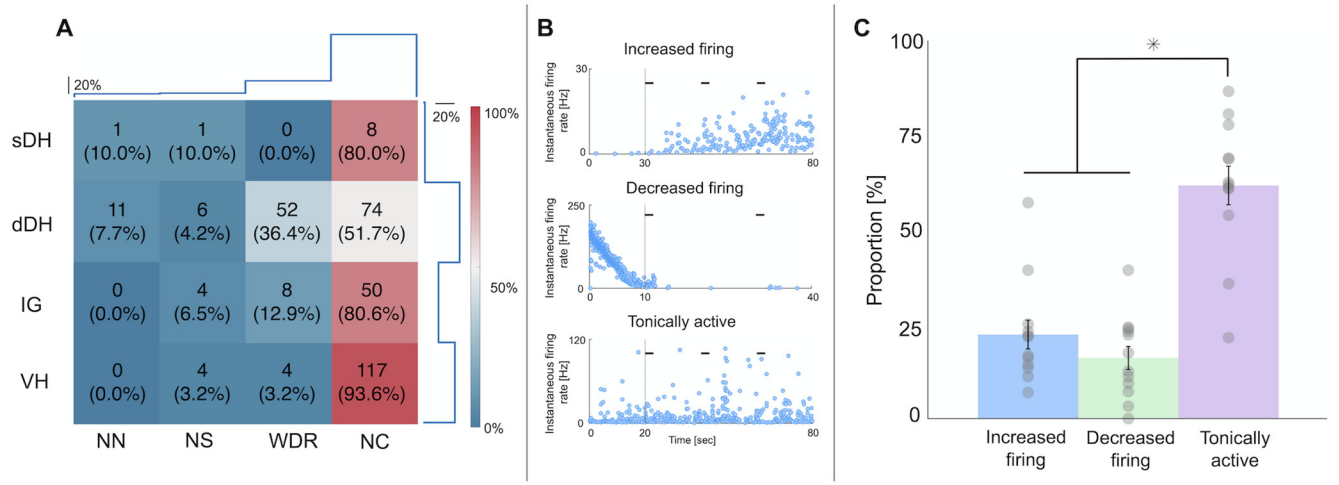

Figure 7. Induced sensory feedback reveals the presence of ongoing multimodal neural transmission in spAP. ***A***, Phenomenological classification of neurons exhibiting spAP. NN: non-nociceptive (i.e., responsive only to innocuous mechanical stimulation); NS: nociceptive specific (responsive only to noxious mechanical stimulation); WDR: wide dynamic range (i.e., responsive to innocuous and noxious stimulation); and NC: not classified (i.e., neurons active during sensory transmission not categorized as NN, NS, or WDR). Stair plot on top depicts the percentage of each neuron subgroup across all anatomic regions (sum of columns); stair plot on right depicts the total percentage of active neurons in each anatomic region during cutaneous stimulation, regardless of subgroup (sum of rows). The dDH exhibited the highest prevalence of neurons whose firing rate was predictably modulated during mechanical probing of the dermatome. ***B***, Instantaneous firing rates of three individual VH neurons classified as NC in the previous scheme (i.e., as in ***A***), here reclassified as having an increased firing rate (top), decreased firing rate (middle), or tonic activity (bottom). Vertical dotted lines represent onset of an epoch in which noxious mechanical stimuli were delivered, and horizontal black hashes indicate specific periods of stimulation. ***C***, Proportion of qualitative firing rate changes in IG/VH neurons firing during nociceptive neural transmission (mean ± SEM; $n = 11$, gray dots; overall main effect of firing type subgroup, $F = 33.994$, $p \ll 0.001$, $\eta^2 = 0.673$; tonically active > increased and decreased firing subgroups, both $p \ll 0.001$; no difference between increased and decreased subgroups, $p = 0.949$). Approximately 38% of active IG/VH neurons exhibited a qualitative change in firing rate during nociceptive neural transmission.

firing rate increased during both innocuous and noxious stimulation; or nociceptive specific (NS) if firing rate increased only during noxious stimulation. Neurons with firing dynamics not corresponding to one of these categories were considered to be non-classified (NC) in this scheme. We were able to reliably track 340 neurons across five of the 11 animals in the initial spAP cohort, averaging 68 ± 6 neurons per animal during these mixed spAP and cutaneous stimulation trials. The anatomic distribution of all active neurons per animal, independent of phenomenological type, was as following: sDH, 2 ± 1 (~3%); dDH, 29 ± 5 (~42%); IG, 12 ± 1 (~18%); and VH, 25 ± 1 (~37%; Fig. 7*A*, staircase plot on right side of heatmap).

We found that spontaneously active neurons included each of the above phenomenological types, indicative of clear multimodal neural transmission. The average number of neurons by phenomenological type per animal was (in descending order of prevalence) as following: NC, 50 ± 2 (~73%); WDR, 13 ± 4 (~19%); NS, 3 ± 1 (~4%); and NN, 2 ± 1 (~4%; Fig. 7*A*, staircase plot on top of heatmap). However, anatomic differences in the distribution of classified neurons were also evident (Fig. 7*A*). For example, the dDH exhibited the highest prevalence of neurons whose firing rate was predictably modulated during mechanical probing of the dermatome, presumably related to its possession of ~81% of identified WDR neurons, ~92% of NN neurons, and ~40% of NS neurons. The VH, by comparison, contained the highest proportion of NC neurons, both relative to other types of neurons in the same region (93.6%) and as a percentage of the total number of NC neurons across all regions (~47%). No rat-level subgroups were found (rat-level variance in linear mixed model ≪0.001; Wald's Z not calculated).

From these results, it is not possible to determine unequivocally if the observed VH neural transmission reflects spAP in premotor interneurons, motoneurons, other interneurons intercalated among the crural flexor motor pools. The most likely scenario would be spAP in a mixture of interneuron types, both because somatic motoneurons are not currently understood to exhibit true spAP in the mature spinal cord and because we did not observe systematic differences in spAP between the lateral and medial electrode shanks (the medial shank did not routinely terminate in a motor pool). This interpretation is supported by the predominance of NC neurons in the VH and the diminished flexion-withdrawal reflexes under anesthesia.

Unconscious, multimodal spAP is behaviorally relevant

A particularly intriguing finding was the relatively high proportion of spiking neurons in the IG and VH during periods of nociceptive neural transmission. Indeed, more than half of all spiking neurons were located in these regions (~55%, including NS, WDR and NC neurons; Fig. 7*A*). The presence of NS and WDR neurons in these regions, although somewhat modest compared with the dDH, suggested that a portion of the multimodal spAP documented above could reflect latent transmission in sensorimotor reflex circuits, for example flexion-withdrawal reflex pathways. However, the strict classification scheme above also led to categorization of nearly half of the active IG/VH neurons as NC. As a result, the extent to which their firing dynamics were modulated during nociceptive transmission was not immediately clear.

To address this outstanding question, we conducted an additional, qualitative analysis of each spike train in the IG/VH specifically during noxious stimulation of the dermatome. This analysis was cross-sectional, in that neurons were not tracked across other stimulation modalities or trials. As a result, data are drawn from 287 IG/VH neurons across 12 animals, including the 187 neurons defined above as NS, WDR, and NC in the IG and VH.

Each neuron was grouped into one of the following categories, broadly reflective of its firing rate during periods of nociceptive neural transmission: increased, decreased, or tonically active. The increased category included neurons that were either recruited or increased their firing rate during nociceptive transmission, as well as neurons already classified as NS or WDR (Fig.

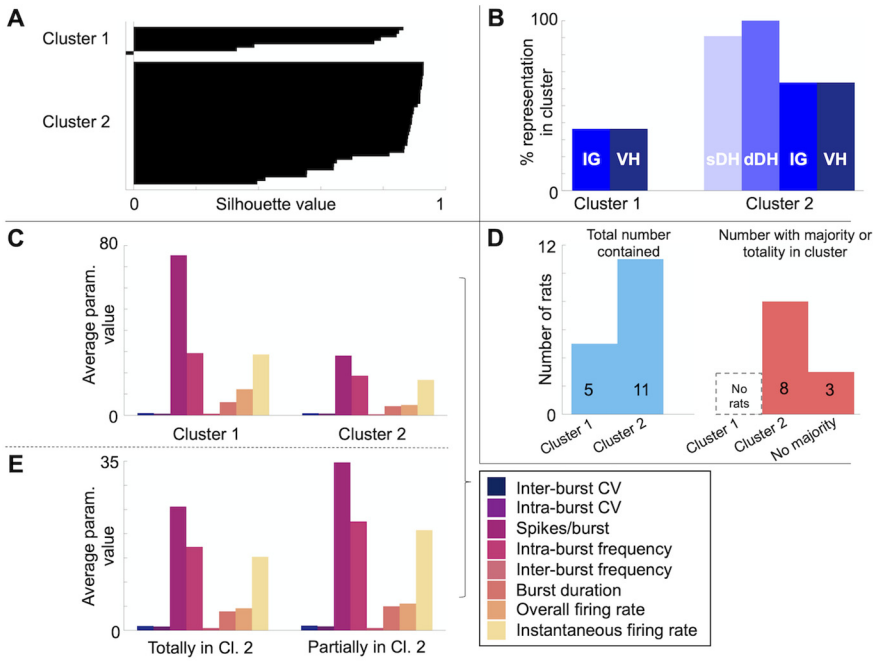

Figure 8. Cluster analysis reveals no rat-level subgroups in spontaneously bursting neurons. ***A***, Bursting neurons formed two well delineated clusters when considering all firing properties. ***B***, Cluster 1 contained no neurons in the sDH or dDH, while cluster 2 contained neurons in all regions. ***C***, Separation between the two clusters appears to have been driven primarily by higher firing rate metrics in cluster 1. ***D***, blue bars, left, Although cluster 2 contained more rats than cluster 1, all rats in cluster 1 were also represented in cluster 2. Red bars, right, All or a majority of the parameters for 8/11 rats were captured by cluster 2. ***E***, No systematic differences are evident between rats whose parameters are fully contained in cluster 2 versus those with only partial representation in cluster 2.

7*B*, top panel); the decreased category included neurons that were derecruited or decreased their firing rate during periods of nociceptive transmission (Fig. 7*B*, middle panel); and the tonically active category included both (1) neurons in which neither clear increases nor decreases in firing rate were evident during periods of nociceptive transmission and (2) bursting neurons whose bursts were not synchronous with periods of nociceptive transmission (Fig. 7*B*, bottom panel). On average, 38% of IG/VH neurons exhibited clear increases or decreases in firing rate during epochs containing noxious cutaneous stimulation (Fig. 7*C*). Per animal, this translated to 9 ± 2 IG/VH neurons exhibiting changes in firing rate versus 15 ± 2 IG/VH neurons that did not. Of those neurons that did exhibit a change, firing rate increased in ~21% and decreased in ~15% (overall main effect of firing type subgroup, $F = 33.994$; $p \ll 0.001$; $\eta^2 = 0.673$; tonically active $>$ increased and decreased firing subgroups, respectively, both $p \ll 0.001$; no difference between increased and decreased subgroups, $p = 0.949$; rat-level variance in linear mixed model $\ll 0.001$, Wald's Z not calculated).

Unconscious spAP is not explained by rat-level subgroups

Although the subgroup analyses above and the relatively precise estimates of mean parameter values strongly implied that rat-level factors were not a significant component of our results, it was possible that rat-level subgroups could have emerged when investigating higher-order associations between variables (i.e., 3, 4, 5, etc., parameters). Traditional mixed modeling approaches are not well suited to characterization of these potential interrelationships in our dataset because it is not possible to unambiguously classify many of our parameters as independent variables, dependent variables, or covariates. Given these modeling considerations, we performed a cluster analysis on the bursting neuron data (which comprised the overwhelming majority of the observed neurons across all regions; Fig. 4*A*,*C*).

The analysis revealed two well-delineated clusters in the multidimensional data (mean silhouette value of 0.78; Fig. 8*A*). Clustering fidelity decreased with three, four, or five clusters, as evidenced by lower mean silhouette values (0.68, 0.63, and 0.62, respectively). Note that in Figure 8*A*, the negative silhouette value in cluster 1 corresponds to the sDH for one rat, which contained no spontaneously bursting neurons and therefore had no firing rate parameters to estimate. In Figure 8*B*, we present the distribution of anatomic regions in each cluster, expressed as a percentage of all animals. For example, cluster 2 contained all of the sDH and dDH bursting neurons across all animals (note again the one animal in which no bursting neurons were present in the sDH, resulting in the 91% representation of sDH neurons in cluster 2, or 10/11 rats, as opposed to 100%); by extension, cluster 1 contained none.

In Figure 8*C*, we show the distribution of average values for each parameter in the two clusters (pooling across all rats within each cluster and anatomic region). Separation between the two clusters appears to have been driven primarily by firing rate, with greater mean spikes/burst, intraburst frequency, and overall mean instantaneous firing rate in cluster 1 neurons than cluster 2 neurons.

We then asked whether these clusters constituted discrete subgroups of rats. In the blue bars of Figure 8*D*, we show the literal number of rats represented in each cluster. Cluster 1 contains data from five animals and cluster 2 contains data from all 11 animals. Thus, it can be seen that there are no truly discrete rat-level and cluster-level subgroups based on clustering across all parameters.

Given that the interrelationships between the measured parameters are likely to be complex, however, we next asked whether rat-level subgroups could more readily be identified based on whether a given rat had either a totality or a majority of their parameters in a single cluster. These data are shown in the red bars of Figure 8*D*. We find that no rats had a totality or majority of their parameters isolated into cluster 1, whereas eight rats had a majority or totality in cluster 2. Two rats were evenly divided across the clusters, and the aforementioned rat lacking sDH bursting neurons remained NC (although its representation would either be divided evenly between the two clusters or have a majority in cluster 1 based on its parameter estimates in the dDH, IG, and VH, for which spontaneously bursting neurons were evident). In total, 5/11 rats were represented in both clusters, while the remaining 6/11 rats were located totally in cluster 2.

Looking just at cluster 2, we computed the average parameter values for the six rats totally contained in cluster 2 and the remaining five rats (Fig. 8*E*). Qualitatively, the two groups exhibit similar parameter profiles, with the largest apparent difference being that rats only partially represented in cluster 2 exhibit more spikes per burst on average than rats totally represented by

cluster 2. This observation is consistent with the overall distinction between clusters 1 and 2, in which cluster 1 neurons discharge a greater number of spikes per burst, and does not reveal strong additional rat-level subgroups.

Discussion

Our primary findings are: (1) spAP is concurrently present in the sDH, dDH, IG, and VH of the adult spinal cord, with a diverse yet strikingly consistent mixture of neuron types within each region; (2) the proportion of neurons exhibiting spAP in deeper, sensorimotor integrative regions is comparable to that in more superficial, sensory-dominant regions; (3) firing rate, but not spike train variability, varies systematically with region; and (4) spAP includes multimodal neural transmission consistent with executing specific behaviors. These results could indicate that spinal networks remain primed for mediating sensorimotor behaviors during unconsciousness.

Regional distribution of spAP

We hypothesized that spAP could support an intrinsic state of readiness to execute sensorimotor behaviors. Alternatively, spAP could merely reflect a non-salient, baseline level of sensation. We reasoned that a precondition for readiness would be the presence of spAP in both sensory-dominant and motor-dominant networks. Conversely, an increased prevalence of spAP in the sDH and dDH compared with regions where sensorimotor integrative and motor networks are prevalent would be more consistent with spAP primarily reflecting low-level tonic afferent input (Burke et al., 1988; Knellwolf et al., 2019).

We found robust spAP in the DH overall, with the dDH in particular containing the highest proportion of active neurons of any region (~45%). This finding alone would support the interpretation of tonic afferent input driving spAP. However, the dDH is also the largest anatomic region in our preparation by number of electrodes. Taking this difference into account, the prevalence of spAP in the IG/VH is approximately double that of the sDH/dDH. And although afferent-driven transmission is unlikely to be absent entirely, its presence is not incompatible with maintenance of an intrinsic ready state; rather, studies of awake, behaving animals suggest that it may be integral (Prut et al., 2001; Prut and Perlmutter, 2003; Seki et al., 2003, 2009; Cohen and Castro-Alamancos, 2010).

spAP and multimodal transmission, firing type subgroups

It is well accepted that simultaneous activity among an interconnected population of biophysically and functionally diverse neurons is required to mediate the complex sensory and motor processes emblematic of spinal networks. Thus, we reasoned that identification of several neuron subgroups exhibiting spAP within a given region could indicate that such multimodal neural transmission persists during unconsciousness. We took a two-fold approach to addressing this issue, defining neuron subgroups by firing type and by their phenomenological response(s) to sensory transmission (see below, spAP and multimodal transmission, phenomenological subgroups). Classification of neuron subgroups yielded several unexpected findings.

First, each region of the gray matter contained all of the subgroups defined by firing type. The breadth of co-active subgroups could reflect transmission of multiple modes of information (Gerstner et al., 1997; Izhikevich et al., 2003; Thaweerattanasinp et al., 2016), communication between multiple neuron types, or both. Each of these scenarios could be advantageous for maintenance of an intrinsic ready state. And although the apparent lack of simple firing subgroups in the sDH was unexpected (Cervero et al., 1979; Sandkühler and Eblen-Zajjur, 1994; Roza et al., 2016; Lucas-Romero et al., 2018), its compact dimensions, small cell bodies, and proximity to the electrode insertion site likely reduced our yield.

It was also surprising that each region of the gray matter contained a strikingly similar mixture of subgroups. Although the subgroups intentionally captured many common firing types, there was no a priori reason to suspect that the relative mixture would be indistinguishable within each region. Reconciliation of this finding with the literature is difficult, both because previous reports have studied restricted anatomic regions and because methodological differences preclude direct comparisons of absolute neuron quantities (Cervero et al., 1979; Rudomin et al., 1987; Surmeier et al., 1989; Bolton et al., 1991; Sandkühler and Eblen-Zajjur, 1994; McDonagh et al., 1998; Borowska et al., 2013; Medrano et al., 2016; Roza et al., 2016; Lucas-Romero et al., 2018).

One interpretation of the similar neuron mixtures is that it indicates a general, "default" state of sensorimotor readiness. Such a seemingly non-specific state could enhance the salience of synaptic inputs requiring perception and action by leveraging the phenomenon of stochastic resonance (Cordo et al., 1996; Stein et al., 2005; Faisal et al., 2008). That bursting subgroups in particular were disproportionately overrepresented in each region (91% of neurons) could also be taken as evidence of such a state, given that bursting can increase synaptic efficacy over simple firing patterns (Izhikevich et al., 2003; Zeldenrust et al., 2018).

An important remaining question is whether the observed spAP is sufficient to support an intrinsic state of readiness in spinal networks. This would presumably require both an adequate number of active neurons and an appropriate mixture of subgroups. While it is not possible to infer the requisite number, aspects of the observed mixture could potentially be appropriate. Recording from large populations of deep spinal interneurons in monkeys, Prut and Perlmutter (2003) found ~60–70% of spontaneously active neurons were irregular firing at rest before movement onset. Because this spAP occurred before the arrival of corticomotoneuronal volleys or re-afferent feedback, it was taken as evidence of a parallel state of spinal readiness that cooperates with descending motor control to produce behavior (Fetz et al., 2000; Prut et al., 2001; Cohen and Castro-Alamancos, 2010). That we see a comparable proportion of irregular firing neurons in these regions during unconsciousness, without descending drive or vigorous proprioceptive feedback, is consistent with this interpretation.

Neuronal variability in spAP

We expected to find higher average levels of spike train variability in dorsal (sensory) versus ventral (motor) spAP, as is common in supraspinal networks during wakeful behavior (Stein et al., 2005; Faisal et al., 2008). Contrary to our expectation, this was not borne out empirically; CV was insensitive to anatomic region for all subgroups.

This finding could be taken as evidence against the presence of an intrinsic ready state. Indeed, if a function of neuronal variability in sensory networks is to enhance perception via stochastic resonance, it is logical to predict that variability would remain elevated during unconsciousness. However, we also cannot rule out an alternative interpretation consistent with maintenance of a ready state: that intrinsic variability could be increased in

motor networks during unconsciousness because of the lack of a common, synchronous input (i.e., descending drive).

Interestingly, we observed monotonic increases in firing rate metrics with gray matter depth in bursting but not simple firing neurons. This finding may simply reflect localization of neuron populations with different biophysical properties and resonant frequencies. However, intraburst and interburst frequencies are known to modulate synaptic efficacy (Izhikevich et al., 2003; Zeldenrust et al., 2018), raising the possibility that it could be related to differences in the role of spAP across networks.

spAP and multimodal transmission, phenomenological subgroups

We identified 27% of all spontaneously active neurons as either NN, NS, or WDR. Each anatomic region contained $\geq$2/3 of the subgroups, with the dDH containing all three. From these results we can conclude that multimodal neural transmission is indeed a component of spAP. We then reasoned that if a function of spAP is to maintain a state of readiness to execute behaviors, then neurons exhibiting spAP in networks known to execute specific sensorimotor behaviors should transmit the requisite modes of information.

We found that 38% of IG/VH neurons exhibiting spAP also exhibited a clear change in firing rate during induced nociceptive transmission, consistent with flexion-withdrawal reflex circuitry. Thus, at least for this reflex, $>$1/3 of neurons exhibiting spAP appear to be phenomenologically, contextually, and anatomically appropriate for maintaining a ready state. That we found both increases and decreases in firing rate presumably reflects the diverse mixture of neurons in the lumbar enlargement (Gosgnach et al., 2017), including spAP in both excitatory and inhibitory neurons.

Direct evidence for the origin of the observed spAP remains lacking, although it is possible that unstable membrane potentials or intrinsic firing in a subset of neurons drove recurrent firing in broader functional networks, similar to developmental spAP (although the mechanisms are presumably different, e.g., as GABA shifts from excitatory to inhibitory transmission; Blankenship and Feller, 2010). Reduced descending drive could have unmasked latent spAP in some neurons via direct disinhibition, although the net result is difficult to predict given the diverse effects of neuromodulatory inputs on spinal neurons.

Finally, these results are complementary to the recent observation of spontaneous functional connectivity between spinal sensory and motor networks during unconsciousness (McPherson and Bandres, 2021). However, it is possible that stable, well-isolated patterns of neural transmission are not required for maintenance of a ready state. Indeed, there is a growing recognition that transient network architectures are integral to executing precise, repeatable behaviors (Fujisawa et al., 2008; Pham et al., 2020), and it is reasonable to think that dynamic neural assemblies could take on additional importance when specific behaviors are not ongoing.

In conclusion, our results support the notion that unconscious spAP in the adult spinal cord reflects, at least in part, a state of maintained readiness to execute sensorimotor behaviors. While additional verification is warranted, it appears increasingly likely that spAP may be spontaneous in name only.

References

Baccei ML (2014) Pacemaker neurons and the development of nociception. Neuroscientist 20:197–202.

Barry RL, Smith SA, Dula AN, Gore JC (2014) Resting state functional connectivity in the human spinal cord. Elife 3:e02812.

Blankenship AG, Feller MB (2010) Mechanisms underlying spontaneous patterned activity in developing neural circuits. Nat Rev Neurosci 11:18–29.

Bolton PS, Goto T, Wilson VJ (1991) Commissural neurons in the cat upper cervical spinal cord. Neuroreport 2:743–746.

Borowska J, Jones CT, Zhang H, Blacklaws J, Goulding M, Zhang Y (2013) Functional subpopulations of V3 interneurons in the mature mouse spinal cord. J Neurosci 33:18553–18565.

Burke BYD, Gandevia SC, Macefield G (1988) Responses to passive movement of receptors in joint, skin and muscle of the human hand. J Physiol 402:347–361.

Cervero F, Iggo A, Molony V (1979) An electrophysiological study of neurones in the substantia gelatinosa rolandi of the cat's spinal cord. Q J Exp Physiol Cogn Med Sci 64:297–314.

Clement EA, Richard A, Thwaites M, Ailon J, Peters S, Dickson CT (2008) Cyclic and sleep-like spontaneous alternations of brain state under urethane anaesthesia. PLoS One 3:e2004.

Cohen JD, Castro-Alamancos MA (2010) Behavioral state dependency of neural activity and sensory (whisker) responses in superior colliculus. J Neurophysiol 104:1661–1672.

Cordo P, Inglis JT, Verschueren S, Collins JJ, Merfeld DM, Rosenblum S, Buckley S, Moss F (1996) Noise in human muscle spindles. Nature 383:769–770.

Daló NL, Hackman JC (2013) The anesthetic urethane blocks excitatory amino acid responses but not GABA responses in isolated frog spinal cords. J Anesth 27:98–103.

Daniel WW, Cross CL (2013) Biostatistics: a foundation for analysis in the health sciences, Ed 11. Hoboken: Wiley.

De Luca CJ, Erim Z (1994) Common drive of motor units in regulation of muscle force. Trends Neurosci 17:299–305.

Eippert F, Kong Y, Winkler A, Andersson J, Finsterbusch J, Büchel C, Brooks J, Tracey I (2017) Investigating resting-state functional connectivity in the cervical spinal cord at 3T. Neuroimage 147:589–601.

Eschenfelder S, Häbler HJ, Jänig W (2000) Dorsal root section elicits signs of neuropathic pain rather than reversing them in rats with L5 spinal nerve injury. Pain 87:213–219.

Faisal AA, Selen LPJ, Wolpert DM (2008) Noise in the nervous system. Nat Rev Neurosci 9:292–303.

Fetz EE, Perlmutter SI, Prut Y (2000) Functions of mammalian spinal interneurons during movement. Curr Opin Neurobiol 10:699–707.

Fetz EE, Perlmutter SI, Prut Y, Seki K, Votaw S (2002) Roles of primate spinal interneurons in preparation and execution of voluntary hand movement. Brain Res Brain Res Rev 40:53–65.

Fujisawa S, Amarasingham A, Harrison MT, Buzsáki G (2008) Behavior-dependent short-term assembly dynamics in the medial prefrontal cortex. Nat Neurosci 11:823–833.

Gerstner W, Kreiter AK, Markram H, Herz AVM (1997) Neural codes: firing rates and beyond. Proc Natl Acad Sci USA 94:12740–12741.

Gosgnach S, Bikoff JB, Dougherty KJ, El Manira A, Lanuza GM, Zhang Y (2017) Delineating the diversity of spinal interneurons in locomotor circuits. J Neurosci 37:10835–10841.

Grasshoff C, Antkowiak B (2006) Effects of isoflurane and enflurane on GABAA and glycine receptors contribute equally to depressant actions on spinal ventral horn neurones in rats. Br J Anaesth 97:687–694.

Hara K, Harris RA (2002) The anesthetic mechanism of urethane: the effects on neurotransmitter-gated ion channels. Anesth Analg 94:313–318, table of contents.

Inácio AR, Nasretdinov A, Lebedeva J, Khazipov R (2016) Sensory feedback synchronizes motor and sensory neuronal networks in the neonatal rat spinal cord. Nat Commun 7:13060.

Izhikevich EM, Desai NS, Walcott EC, Hoppensteadt FC (2003) Bursts as a unit of neural information: selective communication via resonance. Trends Neurosci 26:161–167.

Kim J, Yao A, Atherley R, Carstens E, Jinks SL, Antognini JF (2007) Neurons in the ventral spinal cord are more depressed by isoflurane, halothane, and propofol than are neurons in the dorsal spinal cord. Anesth Analg 105:1020–1006.

Knellwolf TP, Burton AR, Hammam E, Macefield VG (2019) Firing properties of muscle spindles supplying the intrinsic foot muscles of humans in unloaded and freestanding conditions. J Neurophysiol 121:74–84.

Li J, Baccei ML (2011) Pacemaker neurons within newborn spinal pain circuits. J Neurosci 31:9010–9022.

Lincoln DW (1969) Correlation of unit activity in the hypothalamus with EEG patterns associated with the sleep cycle. Exp Neurol 24:1–18.
Lucas-Romero J, Rivera-Arconada I, Roza C, Lopez-Garcia JA (2018) Origin and classification of spontaneous discharges in mouse superficial dorsal horn neurons. Sci Rep 8:9735.
Luz LL, Szucs P, Safronov BV (2014) Peripherally driven low-threshold inhibitory inputs to lamina I local-circuit and projection neurones: a new circuit for gating pain responses. J Physiol 592:1519–1534.
Maggi CA, Meli A (1986a) Suitability of urethane anesthesia for physiopharmacological investigations. Part 3: other systems and conclusions. Experientia 42:531–537.
Maggi CA, Meli A (1986b) Suitability of urethane anesthesia for physiopharmacological investigations in various systems. Part 2: cardiovascular system. Experientia 42:292–297.
Maggi CA, Meli A (1986c) Suitability of urethane anesthesia for physiopharmacological investigations in various systems Part 1: general considerations. Experientia 42:109–114.
Marcantoni M, Fuchs A, Löw P, Bartsch D, Kiehn O, Bellardita C (2020) Early delivery and prolonged treatment with nimodipine prevents the development of spasticity after spinal cord injury in mice. Sci Transl Med 12:eaay0167.
McDonagh JC, Gorman RB, Gilliam EE, Hornby TG, Reinking RM, Stuart DG (1998) Properties of spinal motoneurons and interneurons in the adult turtle: provisional classification by cluster analysis. J Comp Neurol 400:544–570.
McPherson JG, Bandres MF (2021) Spontaneous neural synchrony links intrinsic spinal sensory and motor networks during unconsciousness. Elife 10:e66308.
Medrano MC, Dhanasobhon D, Yalcin I, Schlichter R, Cordero-Erausquin M (2016) Loss of inhibitory tone on spinal cord dorsal horn spontaneously and nonspontaneously active neurons in a mouse model of neuropathic pain. Pain 157:1432–1442.
Negro F, Muceli S, Castronovo AM, Holobar A, Farina D (2016) Multi-channel intramuscular and surface EMG decomposition by convolutive blind source separation. J Neural Eng 13:026027.
O'Donovan MJ, Chub N, Wenner P (1998) Mechanisms of spontaneous activity in developing spinal networks. J Neurobiol 37:131–145.
Pagliardini S, Greer JJ, Funk GD, Dickson CT (2012) State-dependent modulation of breathing in urethane-anesthetized rats. J Neurosci 32:11259–11270.
Pham BN, Luo J, Anand H, Kola O, Salcedo P, Nguyen C, Gaunt S, Zhong H, Garfinkel A, Tillakaratne N, Reggie Edgerton V (2020) Redundancy and multifunctionality among spinal locomotor networks. J Neurophysiol 124:1469–1479.
Prut Y, Perlmutter SI (2003) Firing properties of spinal interneurons during voluntary movement. I. State-dependent regularity of firing. J Neurosci 23:9600–9610.
Prut Y, Perlmutter SI, Fetz EE (2001) Distributed processing in the motor system: spinal cord perspective. Prog Brain Res 130:267–278.
Quiroga RQ, Nadasdy Z, Ben-Shaul Y (2004) Unsupervised spike detection and sorting with wavelets and superparamagnetic clustering. Neural Comput 16:1661–1687.
Rees A, Sarbaz A, Malmierca MS, Le Beau FEN (1997) Regularity of firing of neurons in the inferior colliculus. J Neurophysiol 77:2945–2965.
Roza C, Mazo I, Rivera-Arconada I, Cisneros E, Alayón I, López-García JA (2016) Analysis of spontaneous activity of superficial dorsal horn neurons in vitro: neuropathy-induced changes. Pflugers Arch Eur J Physiol 468:2017–2030.
Rudomin P, Solodkin M, Jiménez I (1987) Synaptic potentials of primary afferent fibers and motoneurons evoked by single intermediate nucleus interneurons in the cat spinal cord. J Neurophysiol 57:1288–1313.
Sandkühler J, Eblen-Zajjur AA (1994) Identification and characterization of rhythmic nociceptive and non-nociceptive spinal dorsal horn neurons in the rat. Neuroscience 61:991–1006.
Seki K, Perlmutter SI, Fetz EE (2003) Sensory input to primate spinal cord is presynaptically inhibited during voluntary movement. Nat Neurosci 6:1309–1316.
Seki K, Perlmutter SI, Fetz EE (2009) Task-dependent modulation of primary afferent depolarization in cervical spinal cord of monkeys performing an instructed delay task. J Neurophysiol 102:85–99.
Steedman WM, Zachary S (1990) Characteristics of background and evoked discharges of multireceptive neurons in lumbar spinal cord of cat. J Neurophysiol 63:1–15.
Stein RB, Gossen ER, Jones KE (2005) Neuronal variability: noise or part of the signal? Nat Rev Neurosci 6:389–397.
Steriade M, Nunez A, Amzica F (1993) A novel slow ($<$ 1 Hz) oscillation of neocortical neurons in vivo: depolarizing and hyperpolarizing components. J Neurosci 13:3252–3265.
Stevens CF, Zador AM (1998) Input synchrony and the irregular firing of cortical neurons. Nat Neurosci 1:210–217.
Surmeier DJ, Honda CN, Willis WD (1989) Patterns of spontaneous discharge in primate spinothalamic neurons. J Neurophysiol 61:106–115.
Svirskis G, Rinzel J (2000) Influence of temporal correlation of synaptic input on the rate and variability of firing in neurons. Biophys J 79:629–637.
Thaweerattanasinp T, Heckman CJ, Tysseling VM (2016) Firing characteristics of deep dorsal horn neurons after acute spinal transection during administration of agonists for 5-HT1B/1D and NMDA receptors. J Neurophysiol 116:1644–1653.
Thaweerattanasinp T, Birch D, Jiang MC, Tresch MC, Bennett DJ, Heckman CJ, Tysseling VM (2020) Bursting interneurons in the deep dorsal horn develop increased excitability and sensitivity to serotonin after chronic spinal injury. J Neurophysiol 123:1657–1670.
Wakai A, Kohno T, Yamakura T, Okamoto M, Ataka T, Baba H (2005) Action of isoflurane on the substantia gelatinosa neurons of the adult rat spinal cord. Anesthesiology 102:379–386.
Wu TL, Yang PF, Wang F, Shi Z, Mishra A, Wu R, Chen LM, Gore JC (2019) Intrinsic functional architecture of the non-human primate spinal cord derived from fMRI and electrophysiology. Nat Commun 10:1416.
Zeldenrust F, Wadman WJ, Englitz B (2018) Neural coding with bursts—current state and future perspectives. Front Comput Neurosci 12:48.
Zhurakovskaya E, Paasonen J, Shatillo A, Lipponen A, Salo R, Aliev R, Tanila H, Gröhn O (2016) Global functional connectivity differences between sleep-like states in urethane anesthetized rats measured by fMRI. PLoS One 11:e0155343.
Zhurakovskaya E, Leikas J, Pirttimäki T, Mon FC, Gynther M, Aliev R, Rantamäki T, Tanila H, Forsberg MM, Gröhn O, Paasonen J, Jalkanen AJ (2019) Sleep-state dependent alterations in brain functional connectivity under urethane anesthesia in a rat model of early-stage Parkinson's disease. eNeuro 6:ENEURO.0456-18.2019.